Applied Energy 175 (2016) 128–140

Contents lists available at ScienceDirect

Applied Energy

journal homepage: www.elsevier.com/locate/apenergy

A comparison and accuracy analysis of impedance-based temperature estimation methods for Li-ion batteries ☆

H.P.G.J. Beelen [a,*], L.H.J. Raijmakers [a,c], M.C.F. Donkers [a], P.H.L. Notten [a,b], H.J. Bergveld [a,d]

[a] Dept. Electrical Engineering, Eindhoven University of Technology, Netherlands
[b] Dept. Fundamental Electrochemistry, Forschungszentrum Jülich, Germany
[c] Dept. Radiation, Science and Technology, Delft University of Technology, Netherlands
[d] NXP Semiconductors, Eindhoven, Netherlands

HIGHLIGHTS

- Temperature and State-of-Charge sensitivity analyses of the battery impedance.
- New framework for capturing existing EIS-based temperature estimation methods.
- Comparison and analysis of EIS-based temperature estimation, using this framework.
- Compared to existing methods, a more-accurate EIS-based method is synthesised.

ARTICLE INFO

Article history:
Received 5 February 2016
Received in revised form 30 March 2016
Accepted 24 April 2016
Available online 6 May 2016

Keywords:
Lithium-ion batteries
Electrochemical Impedance Spectroscopy
Battery temperature
Monte-Carlo simulations

ABSTRACT

In order to guarantee safe and proper use of Lithium-ion batteries during operation, an accurate estimate of the battery temperature is of paramount importance. Electrochemical Impedance Spectroscopy (EIS) can be used to estimate the battery temperature and several EIS-based temperature estimation methods have been proposed in the literature. In this paper, we argue that all existing EIS-based methods implicitly distinguish two steps: experiment design and parameter estimation. The former step consists of choosing the excitation frequency and the latter step consists of estimating the battery temperature based on the measured impedance resulting from the chosen excitation. By distinguishing these steps and by performing Monte-Carlo simulations, all existing methods are compared in terms of accuracy (i.e., mean-square error) of the temperature estimate. The results of the comparison show that, due to different choices in the two steps, significant differences in accuracy of the estimate exist. More importantly, by jointly selecting the parameters of the experiment-design and parameter-estimation step, a more-accurate temperature estimate can be obtained. In case of an unknown State-of-Charge, this novel method estimates the temperature with an average absolute bias of 0.4 °C and an average standard deviation of 0.7 °C using a single impedance measurement for the battery under consideration.

1. Introduction

Due to properties such as high energy density, Lithium-ion (Li-ion) batteries are used in various applications such as battery packs in (hybrid) electric vehicles and in mobile phones. For safety and control purposes, temperature estimation of Li-ion batteries is of vital importance. For example, high battery temperatures can induce thermal runaway, which may cause fire or explosions, and accelerate ageing of the battery, thus reducing its lifetime and performance [2,3]. A relatively new field of temperature estimation methods is based on Electrochemical Impedance Spectroscopy (EIS), where a temperature relation is inferred from the electrochemical battery impedance. Using EIS for temperature estimation is often referred to as "sensorless temperature estimation", since no intrusive or surface-mounted temperature sensors are needed. Another advantage is that the average[1] battery temperature is gauged. Therefore, there is no heat transfer delay due to the

☆ Preliminary results of this work have been presented at the 2015 IFAC Workshop on Engine and Powertrain Control, Simulation and Modeling (E-COSM'15) [1].

* Corresponding author at: Department of Electrical Engineering, Eindhoven University of Technology, PO Box 513, 5600 MB Eindhoven, Netherlands.
E-mail address: h.p.g.j.beelen@tue.nl (H.P.G.J. Beelen).

[1] Note that, due to temperature gradients and the non-linear relation between battery impedance and battery temperature, the EIS-based average temperature, which can be interpreted as a weighted average, is not necessarily equal to the actual average temperature. However, these average temperatures will typically be close in value [4].

http://dx.doi.org/10.1016/j.apenergy.2016.04.103
0306-2619/

Nomenclature

EIS	Electrochemical Impedance Spectroscopy	SNR	Signal-to-Noise Ratio
SoC	State-of-Charge	BMS	Battery Management System
MSE	Mean-Square Estimation error		

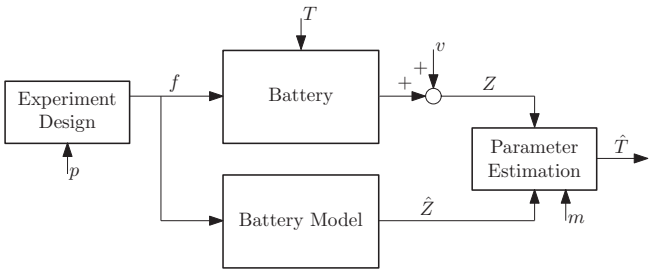

Fig. 1. Top-level block diagram of measurement system.

thermal mass of the battery as with measurements of the surface temperature.

A number of studies have presented EIS-based temperature estimation methods and expansions or improvements of these methods [4–14]. It can be argued that the presented methods can be broken down into two components: how to choose the excitation signal for the battery and how to estimate the battery temperature based on the measured output resulting from the chosen excitation signal. In Fig. 1, a general block diagram is shown that can be used to describe existing EIS-based temperature estimation methods. Here, the frequency f defines the excitation signal and the measured output Z is the battery impedance. Choosing the excitation frequency f is referred to as *experiment design*, whereas estimating the battery temperature based on the measured impedance Z is referred to as *parameter estimation*. The real battery temperature and estimated battery temperature are denoted by T and $\hat{T}$, respectively, and v denotes measurement noise on the measured impedance Z. Furthermore, a battery impedance model is employed to establish a relation between the measured battery impedance Z and the battery temperature T. In Fig. 1, this is captured by the modelled battery impedance $\hat{Z}$, which is computed by using a battery impedance model and the excitation frequency f.

In general, the modelled battery impedance $\hat{Z}$ is compared to the measured battery impedance Z, using some established temperature relation, in order to obtain a temperature estimate $\hat{T}$. This comparison is defined by the *parameter-estimation* component by means of settings given by m. For example, one existing estimation method [7] relates the real part of the battery impedance Z to the battery temperature T. Therefore, the parameter m induces the setting "real part of Z" on the *parameter-estimation* block and the battery temperature T is estimated in the form of $\hat{T}$ by comparing the real part of the measured battery impedance Z to the real part of the modelled battery impedance $\hat{Z}$ at the excitation frequency f. The settings for *experiment design* p should yield a certain frequency f that causes the output Z to have the right information for the *parameter estimation* to give accurate results. For example, a sensitivity analysis in [7] reveals that a high variation of impedance Z with temperature T can be found for low frequencies f. However, also a high variation of the impedance Z with the State-of-Charge (SoC) is found in this frequency region. The combination of both sensitivity analyses can be seen as choosing the *experiment-design* parameter p, which resulted in [7] in a compromise in the excitation frequency f. Also, p can hold information as to how many measurements are taken and averaged in order to obtain a temperature estimate.

In this paper, we compare and analyse the accuracy of impedance-based temperature estimation and propose a method that yields a more accurate temperature estimate, when compared to the existing methods. To do so, we will analyse the sensitivity of the battery impedance with respect to temperature and SoC. Also, we will carefully investigate both *experiment design* and *parameter estimation* of impedance-based temperature estimation by introducing several parameters, and explain how existing methods can be considered as having certain choices for these parameters. A Monte-Carlo approach will be taken to analyse how different choices in *experiment design* and *parameter estimation* will lead to a different accuracy of $\hat{T}$. This accuracy is defined as the Mean-Square Estimation error (MSE) of the temperature estimate $\hat{T}$, where the MSE can be broken down into bias (i.e., systematic error) and standard deviation (i.e., random error) of the temperature estimate $\hat{T}$ (compared to the real battery temperature T). This will allow for a thorough comparison of the achieved estimation accuracy of the state-of-the-art impedance-based temperature estimation methods. Moreover, the analysis allows for synthesising parameters p and m that yield a more accurate temperature estimate (in terms of a smaller MSE value). As a basis for the comparison, analysis and synthesis, a data-based approach is chosen. No prior knowledge about batteries or battery modelling is assumed and therefore this paper focuses on the estimation problem instead of battery modelling and related issues. This makes the framework widely applicable for data-based battery analysis which is an addition to the work in [14], where polynomial modelling is chosen and where a comparison of existing methods is not included. The work presented in this paper extends on preliminary work [1] by performing extensive sensitivity analyses of the battery impedance with respect to temperature and SoC, by giving a more thorough analysis of temperature estimation, a more extensive comparison of estimation methods as well as by pointing to interesting extensions of this work.

The organisation of the paper is as follows. Some theoretical background is presented in Section 2. Then, the principle of impedance-based temperature estimation and the proposed approach for comparison, analysis and synthesis are introduced in Section 3. Subsequently, Section 4 will give an extensive sensitivity analysis of the battery impedance with respect to temperature and SoC. The results of this study are presented and discussed in Section 5 and some possible extensions to this work are discussed in Section 6. Conclusions are drawn in Section 7.

2. Theoretical background

Let $Z \in \mathbb{C}$ denote a complex number of the form $Z = a + jb$ where $a, b \in \mathbb{R}$ and j satisfies $j^2 = -1$. The real and imaginary parts of this complex number are denoted by $\mathrm{Re}(Z) = a$ and $\mathrm{Im}(Z) = b$, respectively. Furthermore, the complex modulus is given by $|Z| = \sqrt{a^2 + b^2}$ and the argument or phase by $\arg(Z) = \arctan(b/a)$.

Let x_i with $i \in \{1, \ldots, N\}$ denote N independent and identically distributed random variables. Then, the sample mean of x is given by

$$M_N(x) = \frac{1}{N}\sum_{i=1}^{N} x_i. \tag{1}$$

For $N \to \infty$, the sample mean $M_N(x)$ converges to the expected value $\mathrm{E}[x]$ of x. The sample variance of x is given by

$$\mathrm{Var}_N(x) = \frac{1}{N}\sum_{i=1}^{N}(x_i - M_N(x))(x_i - M_N(x))^{\intercal}. \tag{2}$$

For $N \to \infty$, the sample variance $\mathrm{Var}_N(x)$ converges to the variance $\sigma^2(x) = \mathrm{E}[(x - \mathrm{E}[x])(x - \mathrm{E}[x])^{\intercal}]$ of x, which equals the square of the standard deviation σ. Around the expected value $\mathrm{E}[x]$ of a random variable x, a confidence interval with confidence β such that $x \in [\underline{x}, \overline{x}]$ is defined as

$$P[\underline{x} \leqslant E[x] \leqslant \overline{x}] \geqslant \beta. \tag{3}$$

In case the upper bound is given by $\overline{x} = M_N(x) + c$, and the lower bound is given by $\underline{x} = M_N(x) - c$, making the length of the confidence interval to be $2c$, then $\beta = 1 - \mathrm{Var}_N[x]/(Nc^2)$. This allows us to calculate the sample size N for a desired confidence interval $2c$ with a certain confidence coefficient β, or to calculate β for a given N.

Furthermore, let $Z = g(T)$ denote a non-linear function, where Z could be the measured impedance in Fig. 1 and $g(T)$ could be the battery model. Then, one way of estimating T is by using a non-linear regression approach, such as non-linear least squares, which can be denoted by $\hat{T} = \arg\min_T \|Z - g(T)\|^2$ where $\|\cdot\|$ is any vector norm. In this paper, we will take the Euclidean norm.

For an uncertain model $g(T)$ that is parametrised by parameter T, a probability distribution $P(Z|T)$, and produces observations Z, the estimate of the parameter T is denoted by $\hat{T}$. The expected value of $\mathrm{E}[\hat{T}]$ is used to define the bias b and the variance of the estimate. When using only a finite number of observations N, Eqs. (1) and (2) can be used instead of $\mathrm{E}[\hat{T}]$ and the variance based on $\mathrm{E}[\hat{T}]$, respectively. Then, bias $b(\hat{T})$ and variance $\mathrm{Var}(\hat{T})$ are given by

$$\mathrm{b}(\hat{T}) = M_N(\hat{T}) - T \quad \text{and} \quad \mathrm{Var}(\hat{T}) = \mathrm{Var}_N(\hat{T}), \tag{4}$$

respectively and the MSE is given by

$$\mathrm{MSE} = \mathrm{b}(\hat{T})^2 + \mathrm{Var}(\hat{T}). \tag{5}$$

Finally, complex-valued zero-mean Gaussian noise is denoted by $v = c + jd$, where the vector $[c\,d]^{\intercal}$ is a (joint) Gaussian distribution with zero mean and variance σ^2.

3. Impedance-based temperature estimation

In this section, an overview of the framework for analysis, comparison and synthesis of impedance-based temperature estimation as presented in [1] will be given. This overview will include the definition of the battery impedance Z, the relation of Z with respect to the battery temperature T and the proposed estimator for accurately estimating T given the aforementioned relation with Z. Furthermore, the framework in [1] will be extended towards the case where accurate information on the SoC is available. Also, the overview of state-of-the-art estimation techniques in [1] will be updated with recent literature.

3.1. Battery impedance modelling

The battery impedance Z can be interpreted as the battery frequency response, where the battery takes a sinusoidal voltage or current input with frequency $f = \omega/(2\pi)$, and produces a sinusoidal current or voltage output, respectively, with the same frequency. The ratio between input and output can be described as a (complex) impedance

$$Z(j\omega) = \frac{V(j\omega)}{I(j\omega)}, \tag{6}$$

where the magnitude of the excitation signal should be sufficiently small in order to guarantee local linearity of the system, yet not too small to prevent a poor Signal-to-Noise Ratio (SNR). The technique of obtaining the frequency response of the battery is known as EIS and is widely used for gathering information about batteries [15–18]. In this study, EIS measurements are conducted in galvanostatic mode by superimposing a sinusoidal current with an amplitude of $100\sqrt{2}$ mA on the load current of the battery (whether or not a load current is present).

As discussed in the introduction, modelling efforts are limited to defining a data-based model instead of using modelling approaches such as first-principles modelling or equivalent-circuit modelling [19,20]. In particular, we model the battery by a function $g : \mathbb{R}^4 \to \mathbb{C}$, that depends on excitation frequency f, temperature T, State-of-Charge (SoC) and other effects w such as battery ageing and (dis)charge current. If also additive measurement noise $v \in \mathbb{C}$, induced by the measurement device, is considered, the battery impedance is given by

$$Z = g(f, T, \mathrm{SoC}, w) + v, \tag{7}$$

where v is complex-valued zero-mean Gaussian noise as introduced in the previous section. In this paper, we do not take into account the dependencies denoted by w and we shall assume $w = 0$ from now on. Still, the parameter w can be used to model other dependencies than f, T and SoC as mentioned above, which can be seen as an extension on this work without changing the approach presented in this paper.

Based on the relation in Eq. (7) and EIS measurements, a battery model can be made, e.g., by storing impedance data in look-up tables. If the measurement noise v and the SoC are assumed to be unknown, for simplicity, a model $\hat{g}$ of the battery impedance Z is constructed by averaging over SoC and v in order to make the model independent of these influences. As a result of these assumptions, the model is given by

$$\hat{g}(f, T) = \frac{1}{KM}\sum_{j=1}^{M}\sum_{i=1}^{K} g(f, T, \mathrm{SoC}_j, 0) + v_i \tag{8}$$

for some $\mathrm{SoC}_j \in [0, 100]$ and $j \in \{1, \ldots, M\}$, where $M \in \mathbb{N}$ is the number of SoC values at which the battery impedance is measured and $K \in \mathbb{N}$ is the number of measurements taken per SoC. The choice and range of SoC values over which is averaged (e.g. $\mathrm{SoC} \in \{40, 60\}$) in order to construct an averaging-based model may depend on the intended application. For example, a battery used in a charge sustaining setup where the SoC is kept around 50% does not require an accurate model for $\mathrm{SoC} \in [0, 100]$, instead, $\mathrm{SoC} \in [40, 60]$ will suffice. In case the SoC is known, e.g., through SoC estimation [21], $\hat{g}$ can be redefined to an SoC-dependent model given by

$$\hat{g}(f, T, \mathrm{SoC}) = \frac{1}{K}\sum_{i=1}^{K} g(f, T, \mathrm{SoC}, 0) + v_i. \tag{9}$$

3.2. Temperature estimation

Fig. 1, Eqs. (8) and (9) show that battery temperature estimation can be broken down into two questions with the joint objective of obtaining the most accurate temperature estimate $\hat{T}$: how to determine the excitation frequency f (or multiple frequencies $f_i, i \in \{1, \ldots, N\}$) and how to obtain the temperature estimate $\hat{T}$ from the measured impedance Z for a certain f? Referring back to Fig. 1, what should p and m be? For answering the first question,

better understanding is needed of the sensitivity of the temperature estimate with respect to the excitation frequency. This will eventually allow us to make a comparison of existing EIS-based estimation methods and it will allow us to devise a more accurate method. The second question has been answered in [1], resulting in the estimator for estimating the battery temperature given by

$$\hat{T}(f,N,\alpha,Z) = \arg\min_{T} \sum_{i=1}^{N} \alpha \bar{g}_1^2(f_i,T,Z_i) + (1-\alpha)\bar{g}_2^2(f_i,T,Z_i), \tag{10}$$

where N is the number of EIS measurements, f is the vector of excitation frequencies $f = [f_1,\ldots,f_N]^\intercal$ with a frequency f_i for each EIS measurement, Z is the vector of measured battery impedance values $Z = [Z_1,\ldots,Z_N]^\intercal$ obtained through EIS, and $\alpha \in [0, 1]$ denotes a selector variable. In Cartesian coordinates, $\bar{g}_1$ and $\bar{g}_2$ are given by

$$\bar{g}_1(f_i,T,Z_i) = \mathrm{Re}(\hat{g}(f_i,T) - Z_i) \tag{11a}$$
$$\bar{g}_2(f_i,T,Z_i) = \mathrm{Im}(\hat{g}(f_i,T) - Z_i) \tag{11b}$$

while for polar coordinates, we have

$$\bar{g}_1(f_i,T,Z_i) = \arg(\hat{g}(f_i,T)) - \arg(Z_i) \tag{12a}$$
$$\bar{g}_2(f_i,T,Z_i) = |\hat{g}(f_i,T)| - |Z_i|. \tag{12b}$$

Note that the model in Eq. (8) is obtained through averaging a number of K EIS measurements, and the result from Eq. (10) is obtained with a number of N EIS measurements using the same model.

The estimator, given in Eq. (10), uses the characterised temperature T in the battery model $\hat{g}(f,T)$, at a certain frequency f, as a decision variable in the minimisation of the difference between the measured impedance Z and the modelled impedance $\hat{g}(f,T)$. At the point where this difference is minimised, the minimiser is taken to be the battery-temperature estimate $\hat{T}$. Furthermore, the physical interpretation for $\alpha = 1$ in Eq. (10) in combination with Eq. (11) is that only $\mathrm{Re}(Z)$ is used in estimating the temperature. For $\alpha = 0$, only $\mathrm{Im}(Z)$ is used. In case Eq. (10) is used in combination with Eq. (12), $\alpha = 1$ can be interpreted as using only $\arg(Z)$ and $\alpha = 0$ as using only $|Z|$.

Now, for given experiment-design settings f and N, the estimation method in Eq. (10) provides a structured approach for comparing, analysing, and finally, improving the parameter-estimation settings, α with a certain coordinate system, Eq. (11) or Eq. (12), for temperature estimation. Providing a framework for improving the parameter-estimation settings, thus deriving a more-accurate estimation method, is a novel contribution of this work. These parameter-estimation settings can be seen as a concrete example of m in Fig. 1. In order to apply an (improved) estimation method with certain settings in f, N and α on a practical application, such as a Battery Management System (BMS), Eq. (10) can be stored as a look-up table which maps the measured input Z to an estimated temperature $\hat{T}$, since all input arguments, except for Z, are fixed in Eq. (10).

3.3. State-of-the-art temperature estimation methods

Currently, there are a number of studies presenting EIS-based temperature estimation methods. In the design of the estimation method, these studies do not clearly differentiate between experiment design and parameter estimation. Table 1 shows the corresponding differentiation as partly presented in [1] of the existing estimation methods. For each method, the estimation parameters f, α and the coordinate system, Eq. (11) or Eq. (12), can be identified to fit Eq. (10). This allows for a comparison of methods in Section 5 for a fixed N.

For a more detailed explanation of the different settings in p and m for the existing temperature-estimation methods, as indicated in Table 1, the reader is referred to [1]. In recent literature, a new method has been presented by Spinner et al. [13], where, contradicting to the methods by Schmidt et al. [7] and Richardson et al. [10], a temperature relation is inferred from $\mathrm{Im}(Z)$ at a fixed frequency rather than from $\mathrm{Re}(Z)$. The estimation parameters for the improved method, which we will propose in Section 5, will be obtained by choosing the estimation parameters which achieve an improved accuracy, in terms of a smaller MSE of the estimated temperature, based on the results of the analysis also presented in Section 5. It should be noted that a better accuracy in terms of MSE is not necessarily equivalent to both a smaller bias and standard deviation since the MSE is given by Eq. (5). A trade-off between bias and standard deviation may also result in a smaller MSE.

4. Sensitivity analysis

The presented estimation method in Eq. (10) in combination with experiment design provides a structured approach for comparing and analysing the accuracy of EIS-based temperature estimation. Also, it provides an approach in finding improved settings in experiment design and parameter estimation. However, which settings should be chosen, and what is the basis for these settings for other state-of-the-art estimation methods? More generally, which p and m are chosen in Fig. 1 and which settings could yield more accurate results? Therefore, an analysis of battery-impedance data may provide indications as to what these settings should be. Also, it may give insight into the choices for certain settings in other studies and their presented estimation methods.

The first condition for obtaining an accurate temperature estimate is that the sensitivity of the battery impedance with respect to temperature should be high. A second condition for an accurate estimate is that the sensitivity with respect to other dependencies such as SoC or w is low. These sensitivities can be clearly shown by approximating the terms in the objective function in Eq. (10) (i.e., $\bar{g}$ in Eq. (11) or Eq. (12)), for a fixed frequency f and for $N = 1$, with a first-order Taylor approximation around the estimated battery temperature $\hat{T}$, i.e.,

$$\begin{aligned}\hat{g}(f,\hat{T}) - g(f,T,\mathrm{SoC},w) - v \\ \approx \frac{\partial g}{\partial T}(\hat{T}-T) + \frac{\partial g}{\partial \mathrm{SoC}}\left(\frac{1}{M}\sum_{j=1}^{M}\mathrm{SoC}_j - \mathrm{SoC}\right) - \frac{\partial g}{\partial w}w - v,\end{aligned} \tag{13}$$

Table 1
Existing temperature-estimation methods.

Method	Experiment-design parameters p	Parameter-estimation parameters m
Schmidt et al. [7]	Fixed f, N	Cartesian, Eq. (11), $\alpha = 1$
Richardson et al. [10]	Fixed f, N	Cartesian, Eq. (11), $\alpha = 1$
Spinner et al. [13]	Fixed f, N	Cartesian, Eq. (11), $\alpha = 0$
Srinivasan [9]	Fixed f, N	Polar, Eq. (12), $\alpha = 1$
Raijmakers et al. [5]	Varying f such that $\mathrm{Im}(Z) = 0$, fixed N	Cartesian, Eq. (11), $\alpha = 0$

where $\hat{g}$ is given by Eq. (8), in which $\frac{1}{K}\sum_{i=1}^{K} v_i \approx 0$ for large enough K.

The sensitivity of the battery impedance with respect to temperature is now given by the partial derivative of g with respect to T. The sensitivity with respect to SoC and w is given by the corresponding partial derivatives. Given the conditions for the sensitivity, we require the partial derivative with respect to T to be large and the other partial derivatives to be small. Therefore, settings for experiment design and parameter estimation should meet these requirements and can be found by inspecting these partial derivatives. Note that this comparison of derivatives is a qualitative comparison since SoC $\in [0, 100]$ and $T \in [-20, 50]$, which are two fundamentally different quantities. As before, it is assumed that $w = 0$.

In Fig. 2a–d, partial derivatives of g with respect to temperature for various parameter-estimation settings (i.e., $\mathrm{Re}(Z), \mathrm{Im}(Z), \arg(Z)$ and $|Z|$) are shown. The measurement setup for obtaining these data will be introduced in Section 5. The horizontal axis of each plot denotes frequency and the vertical axis denotes temperature. The derivative is shown in a colour corresponding to the values in the colourbar. In Fig. 2a and b, the derivatives of $\mathrm{Re}(Z)$ and $\mathrm{Im}(Z)$ with respect to temperature, respectively, are shown. The derivatives of $\arg(Z)$ and $|Z|$ are depicted in Fig. 2c and d, respectively.

For Fig. 2a and b, it can be seen that the largest temperature dependencies can be found in the low frequency range. In this frequency range, the derivative in Fig. 2a significantly decreases above 40 °C and the derivative in Fig. 2b even decreases above 30 °C. It should be noted that, although not visible in the figures due to the maximum value of 17 $\mu\Omega\, K^{-1}$ shown in the contour plots, the derivative in the low-frequency range for Fig. 2b is larger than for Fig. 2a. For measurements at higher frequencies ($>$ 200 Hz) the derivative in Fig. 2a is generally larger than the one in Fig. 2b. In Fig. 2d, where the derivative of the modulus of the battery impedance, $|Z|$, is depicted, similar trends can be observed. A large derivative can be seen in the low frequency range whilst towards the higher frequencies the derivative decreases towards zero. As can be expected, the derivative of the argument with respect to temperature in Fig. 2c shows significantly different behaviour compared to other derivatives. Generally, the mid-range frequencies, 500–1000 Hz, show relatively large dependencies over the full temperature range. In the range of 10–50 °C, lower frequencies up to 500 Hz imply accurate results for a temperature estimate. Besides the temperature dependency, the battery impedance also depends on SoC. Partial derivatives of g, with parameter-estimation settings yielding $\mathrm{Re}(Z)$ and $\mathrm{Im}(Z)$ (i.e., $\alpha = 1$ and $\alpha = 0$, respectively), with respect to SoC are shown in Fig. 2e and f, respectively. Both plots clearly show that the variation of the battery impedance with respect to SoC is quite large for low SoC values, especially for frequencies up to 100 Hz.

In conclusion, the partial derivatives of the sensitivity analyses in Fig. 2 generally indicate that, for low frequencies, the complex battery impedance has a higher sensitivity with respect to temperature and simultaneously, also a higher sensitivity with respect to SoC (especially at low SoC). The existing temperature estimation methods and their corresponding studies as denoted in Table 1 use similar sensitivity analyses, with similar results, in order to select settings for experiment design and parameter estimation. The selection of settings in these studies is typically a quantitative comparison of $\frac{\partial Z}{\partial T}$ and $\frac{\partial Z}{\partial \mathrm{SoC}}$. In other words, a trade-off is found in a large $\frac{\partial Z}{\partial T}$ and a small $\frac{\partial Z}{\partial \mathrm{SoC}}$. However, this trade-off does not take into account how $\frac{\partial Z}{\partial \mathrm{SoC}}$ and $\frac{\partial Z}{\partial T}$ jointly affect the accuracy of the estimated temperature $\hat{T}$. Subsequently, it can be stated that a selection of settings based on the accuracy of the estimated temperature $\hat{T}$, instead of a selection based on a trade-off between $\frac{\partial Z}{\partial T}$ and $\frac{\partial Z}{\partial \mathrm{SoC}}$ (which then results in a certain accuracy of $\hat{T}$), is not considered in existing literature. It can be concluded that selecting settings based on the accuracy of the temperature estimate $\hat{T}$ is not trivial. Therefore, we propose to do a Monte-Carlo study [22], in which the accuracy of the temperature estimate $\hat{T}$ can be evaluated for a range of frequencies f, temperatures T and SoC values, by using a

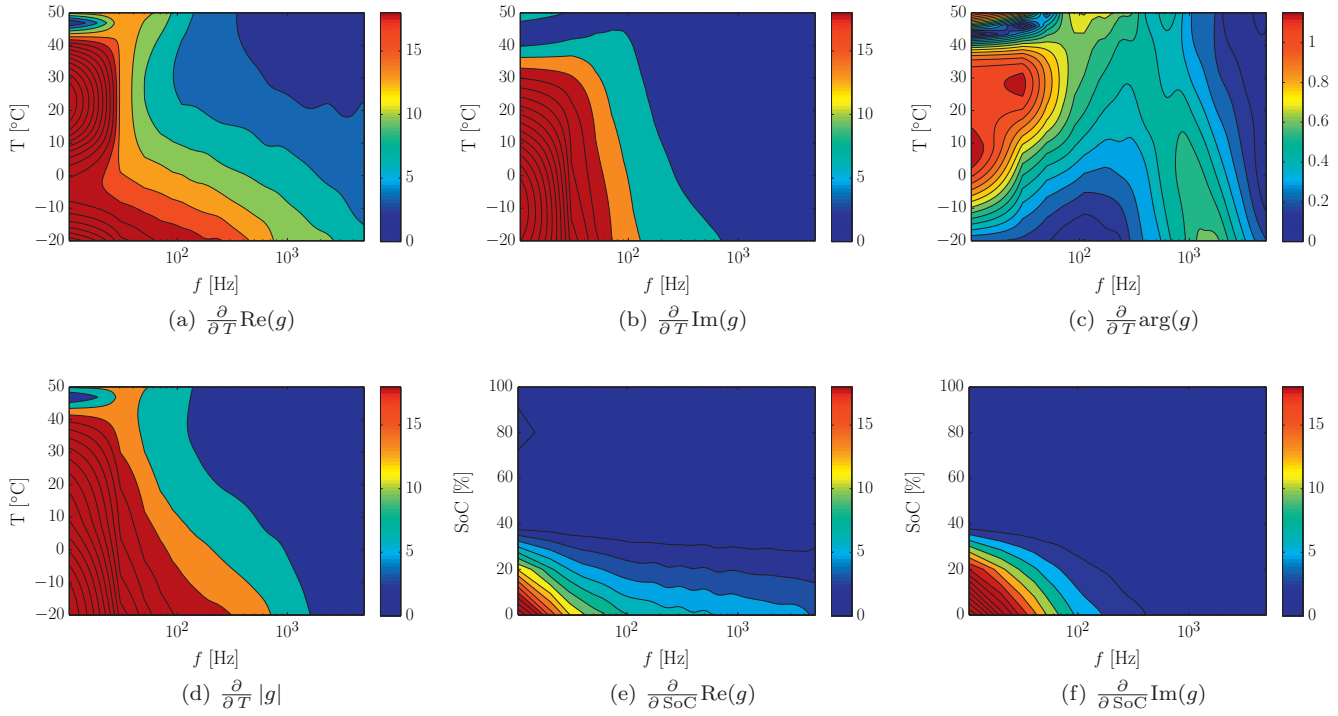

Fig. 2. Subfigures (a)–(d) show partial derivatives at SoC = 40% where (a), (b) and (d) are absolute values in [$\mu\Omega\, K^{-1}$] and (c) is an absolute value in [degree K^{-1}]; subfigures (e) and (f) show partial derivatives in [$\mu\Omega$] at a temperature of $T = 30$ °C.

Table 2
EIS-measurement settings for constructing $\hat{g}$.

Temperature T	$-20, -10, +10, +30, +50$ °C
Frequency f	25 log-spaced f : 10 Hz $\leqslant f \leqslant$ 5 kHz
SoC values	$20, 40, 60, 80\%$

distribution of measured impedance values Z (due to measurement noise v) in Eq. (10) and computing a distribution of temperature estimates $\hat{T}$.

5. Results of accuracy analysis and comparison

To analyse and compare the accuracy of the temperature estimate $\hat{T}$ for existing estimation methods in literature, as well as to synthesise a more accurate estimation method, EIS measurements have been conducted for a single type of battery cell. Based on these measurements and by using Eq. (10), Monte-Carlo simulations have been conducted.

5.1. Comparison of temperature estimation methods

Given foreseeable use of impedance-based temperature estimation in battery packs of (hybrid) electric vehicles, a large-capacity (90 Ah) $LiFePO_4$ cell has been chosen for the experiments. The EIS measurements were conducted with a dedicated measurement setup in combination with Maccor cycling equipment and a climate chamber. The measurement settings for the experiments are given in Table 2, where the real battery temperature T is measured after applying a period of rest in order to reach a thermal equilibrium. The frequency range is based on a lower bound, where the battery impedance becomes SoC-dependent (see Fig. 2e and f). The upper bound is chosen at a frequency where no noticeable temperature dependency is found (see Fig. 2a–d). The temperature range includes temperatures expected during normal operating conditions of battery cells and also, it approximately covers the temperature ranges used in other studies. Temperatures above +50 °C are not considered since the BMS will most likely limit operation or even disconnect the battery when the upper bound of this temperature range is reached due to risk of thermal runaway. Still, temperatures above +50 °C can be estimated, albeit with limited accuracy as can be expected from the trend in Fig. 2, where the sensitivity of the battery impedance with respect to temperature decreases for higher temperatures.

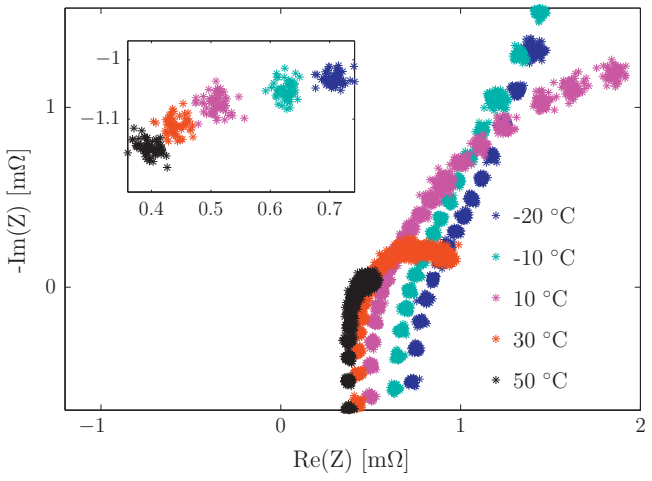

Fig. 3. Nyquist plot of EIS data ($K = 64$) at SoC = 40% at various frequencies and temperatures given in Table 2; inset: EIS measurement data for $f = 2979$ Hz.

For each combination of the measurement settings in Table 2, $K = 64$ measurements have been conducted for $M = 4$ values for SoC. The measurement time for a single impedance measurement was fixed at 1 s, independent of the chosen measurement frequency. In the event of thermal runaway, this will allow for sufficiently fast detection of a rapid rise in temperature. It should be noted that choosing a fixed measurement time provides for an initial averaging of the measurements in the frequency domain, depending on the chosen frequency.

Results from these measurements at SoC = 40% are shown in a Nyquist plot in Fig. 3. Due to the measurement noise v, for each measurement setting, a distribution of $K = 64$ data points can be seen in the Nyquist plot. The inset shows five distributions for five temperatures at a single frequency. Analysis yields that the measurement points are normally distributed with zero mean and a standard deviation in the real and imaginary part of $\sigma = 14$ μΩ. Using the measurement data, a model $\hat{g}$ of the battery impedance can be obtained through Eq. (8). The model comprises a lookup-table with a temperature-frequency grid. A finer temperature-frequency grid than the measurement grid in Table 2 is obtained using spline interpolation.

Finding the temperature estimate requires solving Eq. (10). To evaluate the EIS-based temperature estimation methods, Monte-Carlo simulations are carried out over a range of f, N, α and for Eq. (11) and Eq. (12). The procedure for these Monte-Carlo simulations is as follows. For a certain point in which the accuracy of the temperature estimate $\hat{T}$ is evaluated, i.e., at some f, T, and SoC, an input distribution of measured impedance values Z is generated by adding a distribution of the measurement noise v to the modelled impedance value $\hat{g}$ in Eq. (9), as shown on the left in Fig. 4. For simplicity, only the real part of the impedance, Re(Z), for the input distribution is depicted. The settings for this example are taken to be $f = 100$ Hz, $T = 20$ °C, SoC = 40% and $\alpha = 0.5$. The sample size of the Monte-Carlo simulations (i.e., the number of realisations for Z) is taken $N_{MC} = 10^4$, which results in a $\geqslant$ 95%-confidence bound for temperature estimates being within ±0.2 °C of the actual value,

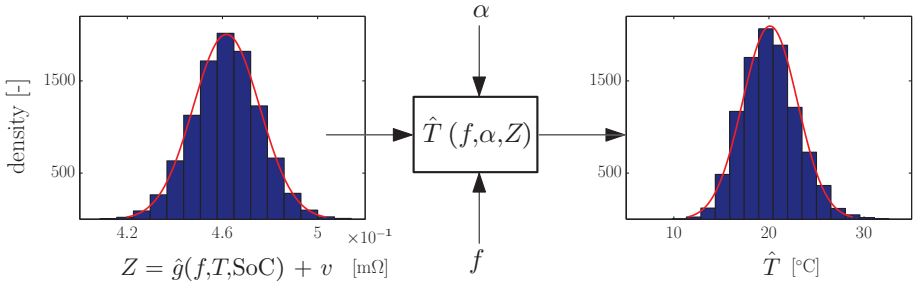

Fig. 4. Illustration of Monte-Carlo simulations. Left: input distribution of impedance values in [mΩ] (where for simplicity only Re(Z) is shown). Right: output distribution of estimated battery temperatures $\hat{T}$ in [°C].

see, e.g., [23]. Eq. (10) is evaluated by inserting the distribution of Z as shown in the centre of Fig. 4. Now, by assessing the output distribution of the Monte-Carlo simulations as shown on the right in Fig. 4, the quality of the temperature estimate $\hat{T}$ can be described in terms of the MSE, see also, e.g., [23]. However, in order to analyse the temperature estimation more thoroughly, we will split the MSE into bias and standard deviation.

The Monte-Carlo simulations allow us to make an assessment of the accuracy of the temperature estimate $\hat{T}$ for any given estimation parameters f, N and α for Eq. (10). Since the existing EIS-based temperature estimation methods [5,7,9,10,13] can all be described by a particular choice for f, N and α and Eq. (11) or Eq. (12), see Table 1, the Monte-Carlo simulations allow the aforementioned methods to be compared. In our comparison and analysis, $N = 1$ is chosen (which leads to a total measurement time of 1 s). Certainly, $N > 1$ will give a smaller estimation error, but it will also take more time to gather measurement data (depending on the chosen measurement frequency f). In order to avoid the discussion on a trade-off between a short measurement time and a small estimation error, we take $N = 1$ in the comparison and analysis. Finally, due to the use of a different battery cell than the ones used in the various studies [5,7,9,10,13], an equivalent excitation frequency f is chosen, satisfying the description of the estimation methods in Section 3.3. Note that for the method of Raijmakers et al. [5], a frequency range is given since they use the concept of zero-intercept frequencies, implying a different frequency for each temperature.

5.2. Analysis of the temperature estimation methods

Figs. 5 and 6 show the results of the analysis of temperature-estimation accuracy, using the model provided in Table 2 for Cartesian and polar coordinates, respectively. Both figures are divided into two blocks of three rows and four columns with contour plots. The horizontal axis in each plot shows the frequency on a logarithmic scale whereas the vertical axis shows the value for α, as in Eq. (10). The colour corresponds to the colourbar to the right of each plot. The first block of each figure shows the bias on the temperature estimate and the second block shows the standard deviation on the estimate in °C. In each block, the columns show SoC values ascending from 20% to 80% and the rows show the real temperatures in ascending order from −10 °C to 30 °C. The accuracy in terms of the MSE can be interpreted as the combination of both blocks (i.e., bias and standard deviation) using Eq. (5). Each block will be discussed separately below.

5.2.1. Bias in Cartesian coordinates

In general, it can be stated that for SoC values towards the edges of the SoC spectrum (e.g. SoC $\in \{20, 80\}\%$) larger differences in bias throughout the contour plot can be seen. Also, this bias is typically larger compared to the centre of the SoC spectrum (e.g. SoC $\in \{40, 60\}\%$). Especially in the high-frequency areas, the bias is larger. For SoC = 20%, the bias at high frequencies towards $\alpha = 0$ is significantly larger than for other points in the plot such as $\alpha = 1$. For SoC = 80%, and towards $\alpha = 1$, this effect seems to be the opposite. In the centre of the SoC spectrum, the deviations in bias throughout the contour plots are smaller than at the edges of the SoC spectrum. However, towards high frequencies, a larger bias can be seen. Moreover, with higher temperatures, this effect is stronger. Given the fact that a model is used that has been averaged over SoC (i.e., Eq. (8) in combination with Table 2), one would expect the bias in the centre of the SoC spectrum to be around zero. Surprisingly, the bias is slightly negative instead (i.e., a light blue colour). A reason for this might be the asymmetry of the battery impedance with respect to SoC (see Fig. 2e and f) in combination with the averaging over SoC. Generally, the lowest bias can be found in the range of 10–300 Hz depending on α. Selection of an α value in this frequency range is less clear and will most likely depend on the analysis of the standard deviation.

5.2.2. Standard deviation in Cartesian coordinates

The standard deviation on the temperature estimate increases substantially for higher temperatures. For different SoC values, no noticeable difference in the standard deviation is present. For $\alpha = 0$, the standard deviation towards higher frequencies is typically larger than for $\alpha = 1$, as can be noticed from the bottom right corner of each plot. Furthermore, all plots are in agreement on the fact that the smallest standard deviation is found for $\alpha = 0.5$, i.e., by equally weighting $\mathrm{Re}(Z)$ and $\mathrm{Im}(Z)$ (which is not equal to using $\alpha = 0$, i.e., $|Z|$, in Eq. (10) with Eq. (12)).

5.2.3. Bias in polar coordinates

The bias plots in polar coordinates in Fig. 6 differ noticeably from the plots in Cartesian coordinates in Fig. 5. This is likely due to the fact that two quantities with different units (i.e., $\arg(Z)$ in radians and $|Z|$ in μΩ) are compared. In all plots, the bias is very large in the bottom right corner, in the high-frequency end where $\alpha = 0$ (i.e., when $|Z|$ is considered). This is in agreement with Fig. 2d, where it can be seen that the sensitivity of $|Z|$ with respect to temperature is near to zero for frequencies above approximately 1 kHz. Furthermore, the contour plots seem to show an irregular pattern. Therefore, we will focus on the cases $\alpha = 0$ and $\alpha = 1$ in order to derive indications for settings of the estimation parameters f and α which should yield a small bias. In terms of frequency ranges, for the case $\alpha = 0$, frequencies up to 500 Hz yield overall a small bias, whereas for the case $\alpha = 1$, defining a frequency range is less clear. For low temperatures, e.g., 10 °C, there are no clear indications for a frequency range which yields a small bias over the entire SoC range at that temperature. This is in agreement with Fig. 2c, where the sensitivity at 10 °C is relatively small compared to higher temperatures. It is debatable which case, $\alpha = 0$ or $\alpha = 1$, performs better with respect to the resulting bias. As for the relation between bias and real battery temperatures, no decisive observations can be made.

5.2.4. Standard deviation in polar coordinates

Also, the plots showing standard deviation differ substantially for polar coordinates in Fig. 6, compared to Cartesian coordinates in Fig. 5. Again, in all plots the bottom right corner shows significantly different behaviour. Here, the standard deviation is relatively large (which is again in agreement with Fig. 2d). Generally it can be seen that, for both $\alpha = 0$ and $\alpha = 1$, the standard deviation is small for low frequencies and increases towards higher frequencies. Especially for higher temperatures, the area of a large standard deviation expands towards lower frequencies. Overall, the frequency range 10–100 Hz gives the best results here. For the case $\alpha = 0$ we can state that frequencies starting from 700 Hz should be avoided.

5.3. Synthesis of an improved estimation method

Besides the use of the framework for comparison and analysis, a novel contribution of this work is the ability to synthesise a more-accurate or improved temperature-estimation method. To do so, the comparison and analysis are used as a roadmap to derive a more-accurate method. The analysis of Figs. 5 and 6 indicates that in Cartesian coordinates, bias and standard deviation increase for higher frequencies and higher temperatures. Overall, frequencies up to 300 Hz are suitable. When a relatively small bias is permitted in order to obtain the smallest standard deviation, the lowest frequency used for these experiments, 10 Hz, should be chosen.

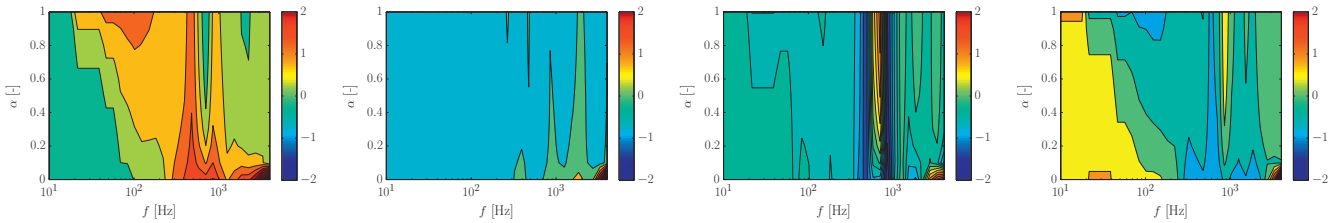

(a) SoC = 20%, $T = -10°C$ (b) SoC = 40%, $T = -10°C$ (c) SoC = 60%, $T = -10°C$ (d) SoC = 80%, $T = -10°C$

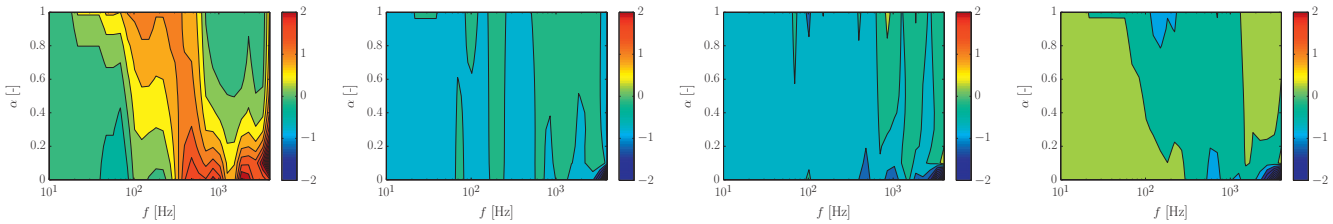

(e) SoC = 20%, $T = 10°C$ (f) SoC = 40%, $T = 10°C$ (g) SoC = 60%, $T = 10°C$ (h) SoC = 80%, $T = 10°C$

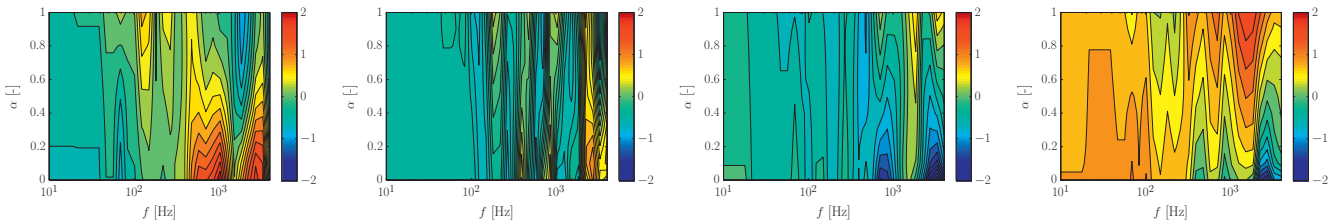

(i) SoC = 20%, $T = 30°C$ (j) SoC = 40%, $T = 30°C$ (k) SoC = 60%, $T = 30°C$ (l) SoC = 80%, $T = 30°C$

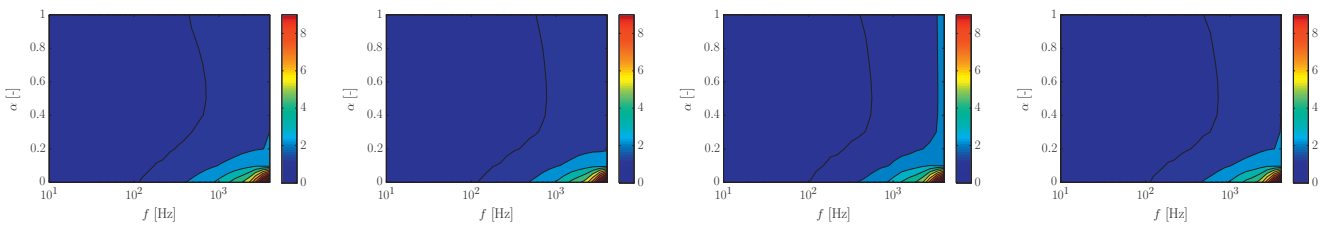

(m) SoC = 20%, $T = -10°C$ (n) SoC = 40%, $T = -10°C$ (o) SoC = 60%, $T = -10°C$ (p) SoC = 80%, $T = -10°C$

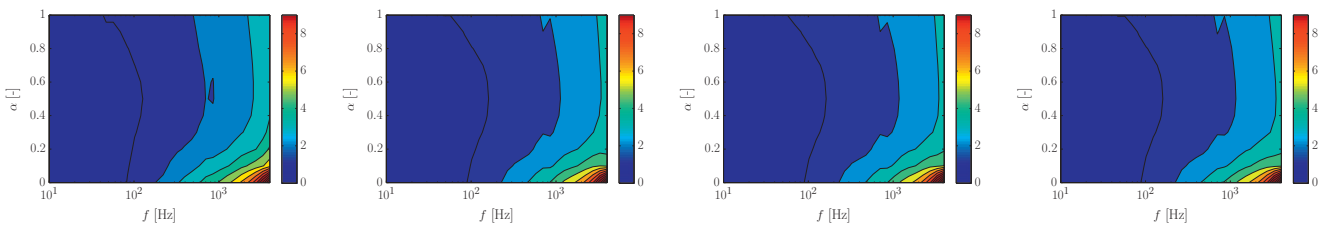

(q) SoC = 20%, $T = 10°C$ (r) SoC = 40%, $T = 10°C$ (s) SoC = 60%, $T = 10°C$ (t) SoC = 80%, $T = 10°C$

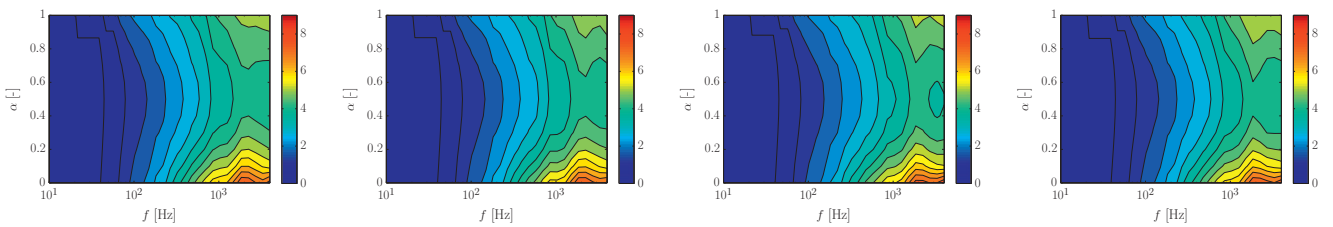

(u) SoC = 20%, $T = 30°C$ (v) SoC = 40%, $T = 30°C$ (w) SoC = 60%, $T = 30°C$ (x) SoC = 80%, $T = 30°C$

Fig. 5. Simulation results with (a)–(l) being the bias and (m)–(x) being the standard deviation (i.e., Eq. (4)) of the temperature estimate $\hat{T}$, respectively. All results are in [°C], given an averaged model over SoC (i.e., Eq. (8)) and in Cartesian coordinates (i.e., Eq. (11)).

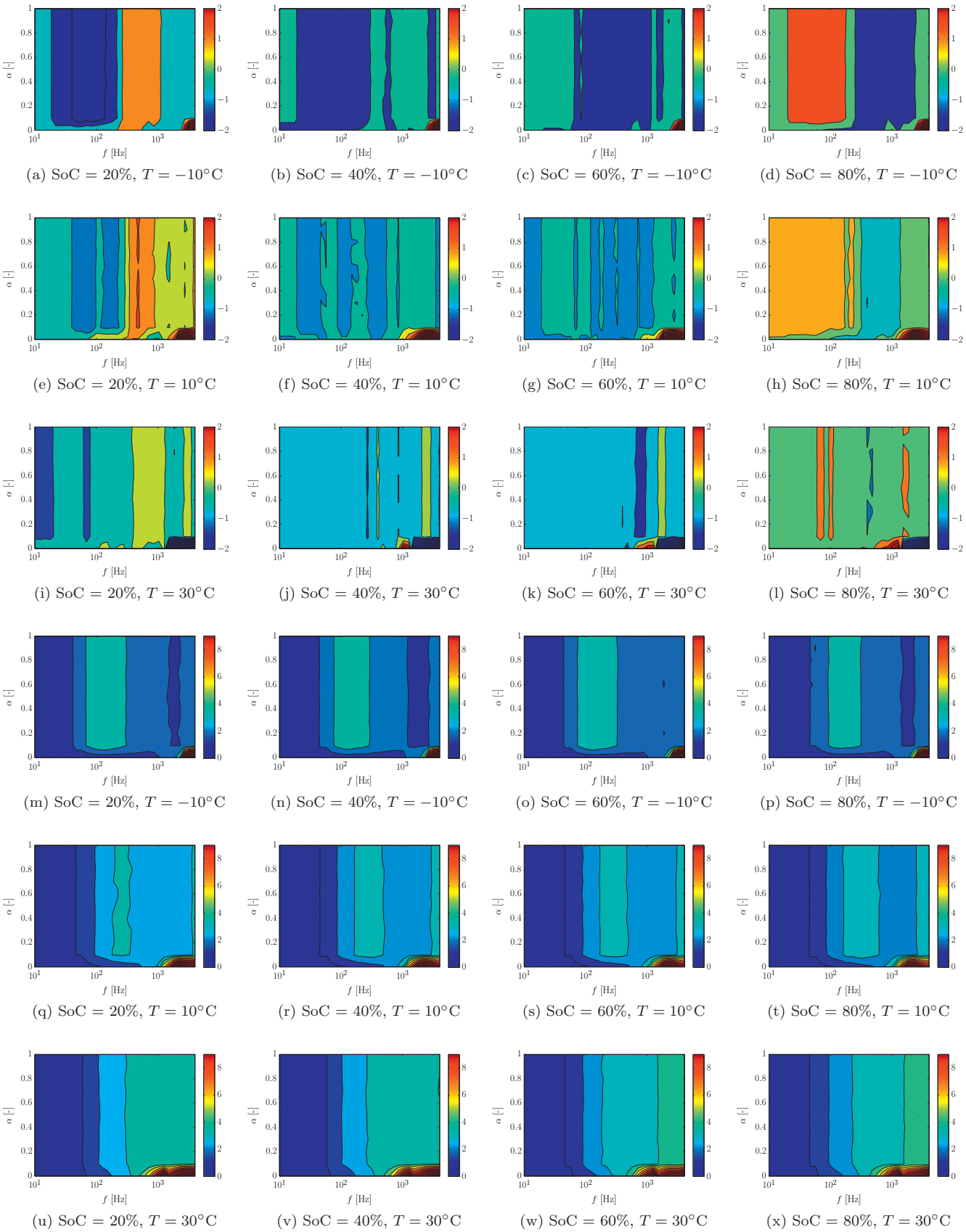

(a) SoC = 20%, $T = -10°C$ (b) SoC = 40%, $T = -10°C$ (c) SoC = 60%, $T = -10°C$ (d) SoC = 80%, $T = -10°C$

(e) SoC = 20%, $T = 10°C$ (f) SoC = 40%, $T = 10°C$ (g) SoC = 60%, $T = 10°C$ (h) SoC = 80%, $T = 10°C$

(i) SoC = 20%, $T = 30°C$ (j) SoC = 40%, $T = 30°C$ (k) SoC = 60%, $T = 30°C$ (l) SoC = 80%, $T = 30°C$

(m) SoC = 20%, $T = -10°C$ (n) SoC = 40%, $T = -10°C$ (o) SoC = 60%, $T = -10°C$ (p) SoC = 80%, $T = -10°C$

(q) SoC = 20%, $T = 10°C$ (r) SoC = 40%, $T = 10°C$ (s) SoC = 60%, $T = 10°C$ (t) SoC = 80%, $T = 10°C$

(u) SoC = 20%, $T = 30°C$ (v) SoC = 40%, $T = 30°C$ (w) SoC = 60%, $T = 30°C$ (x) SoC = 80%, $T = 30°C$

Fig. 6. Simulation results with (a)–(l) being the bias and (m)–(x) being the standard deviation (i.e., Eq. (4)) of the temperature estimate $\hat{T}$, respectively. All results are in [°C], given an averaged model over SoC (i.e., Eq. (8)) and in polar coordinates (i.e., Eq. (12)).

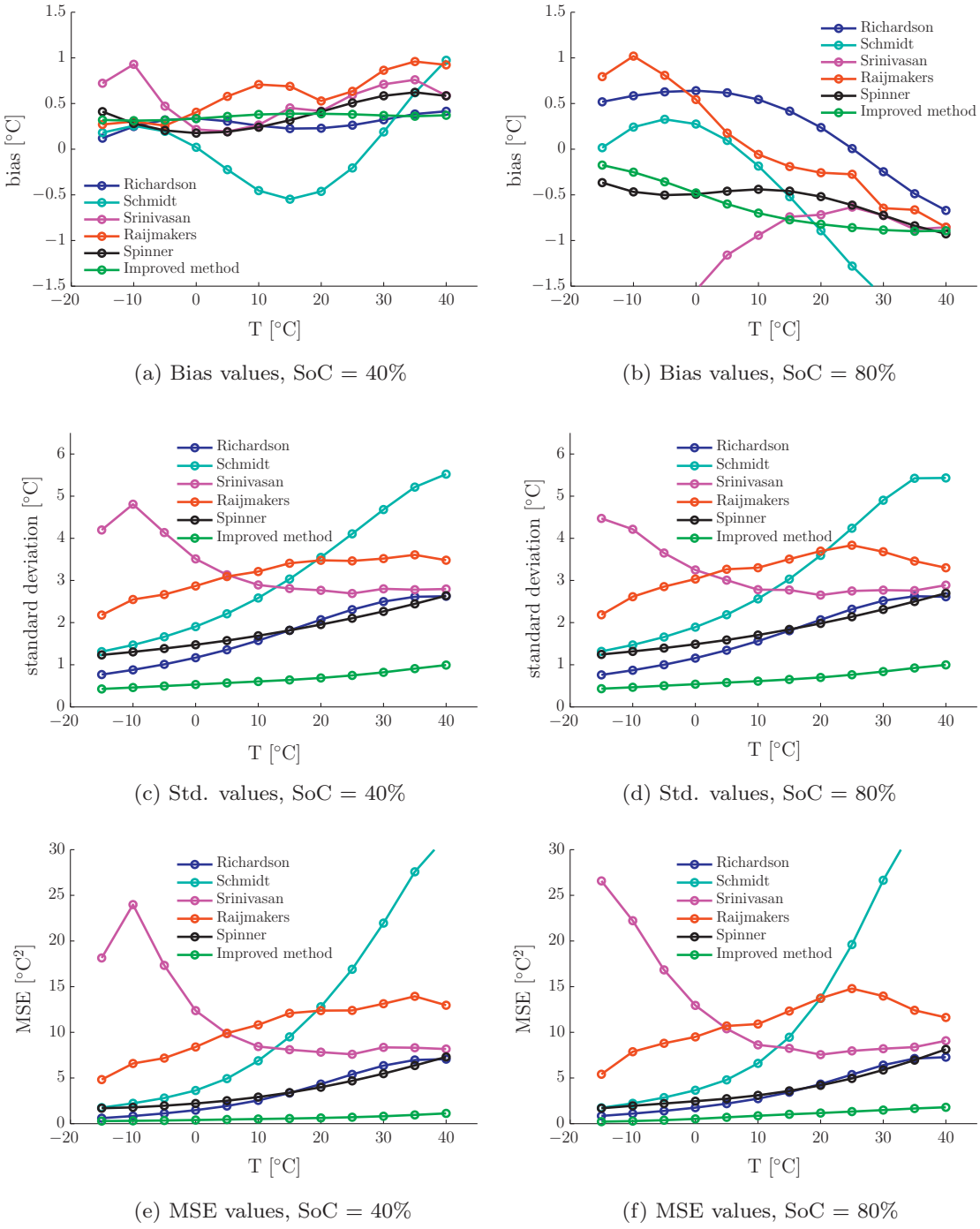

(a) Bias values, SoC = 40%

(b) Bias values, SoC = 80%

(c) Std. values, SoC = 40%

(d) Std. values, SoC = 80%

(e) MSE values, SoC = 40%

(f) MSE values, SoC = 80%

Fig. 7. Results of the comparison of estimation methods for case SoC unknown.

However, the sensitivity analyses in Fig. 2 show that a slightly higher frequency of 50 Hz is preferable since the sensitivity of Re(Z) and Im(Z) with respect to temperature is larger and the sensitivity of Re(Z) and Im(Z) with respect to SoC is smaller. The choice for parameter α is less clear given the analysis for bias, but based on the analysis of standard deviation, we find $\alpha = 0.5$. This is likely due to the fact that for $\alpha = 0.5$, two measurements, Re(Z) and Im(Z), are combined. Indications for values of f and α found in the analysis for polar coordinates are less clear. There, a parameter setting which should be avoided is $\alpha = 0$ in combination with frequencies higher than 300 Hz.

Given the results of the analysis, a new method is proposed, based on Cartesian coordinates. If we accept a small bias in exchange for a small standard deviation we find, for this type of battery cell, estimation parameters $f = 50$ Hz and $\alpha = 0.5$. Note that all conclusions drawn here are specific for the cell under consideration. Still, the proposed methodology and analysis is general and can be extended towards, and repeated for, different battery cells. More precisely, a small-capacity Li-ion cell ($LiCoO_2$, 300 mAh) has also been analysed. Compared to the large-capacity cell under consideration in Fig. 2, similar trends have been observed for the results of the sensitivity analyses. However, given the difference in cell type, it should be noted that, although similar trends were observed, frequency and impedance values corresponding to these trends can be different.

Table 3
Comparison of estimation methods for unknown SoC (case A) and known SoC (case B).

Method	Equivalent f (Hz)	Avg. abs. bias [°C]		MSE [°C^2]		Average σ [°C]
		Case A	Case B	Case A	Case B	Case A & Case B
Schmidt et al. [7]	1300	0.6	0.2	12.1	11.8	3.4
Richardson et al. [10]	150	0.6	0.0	3.8	3.5	1.9
Spinner et al. [13]	150	0.4	0.0	3.8	3.6	1.9
Srinivasan [9]	150	1.0	0.3	12.2	11.5	3.4
Raijmakers et al. [5]	200–650	0.9	0.1	11.0	10.2	3.2
Improved method	50	0.4	0.0	0.7	0.5	0.7

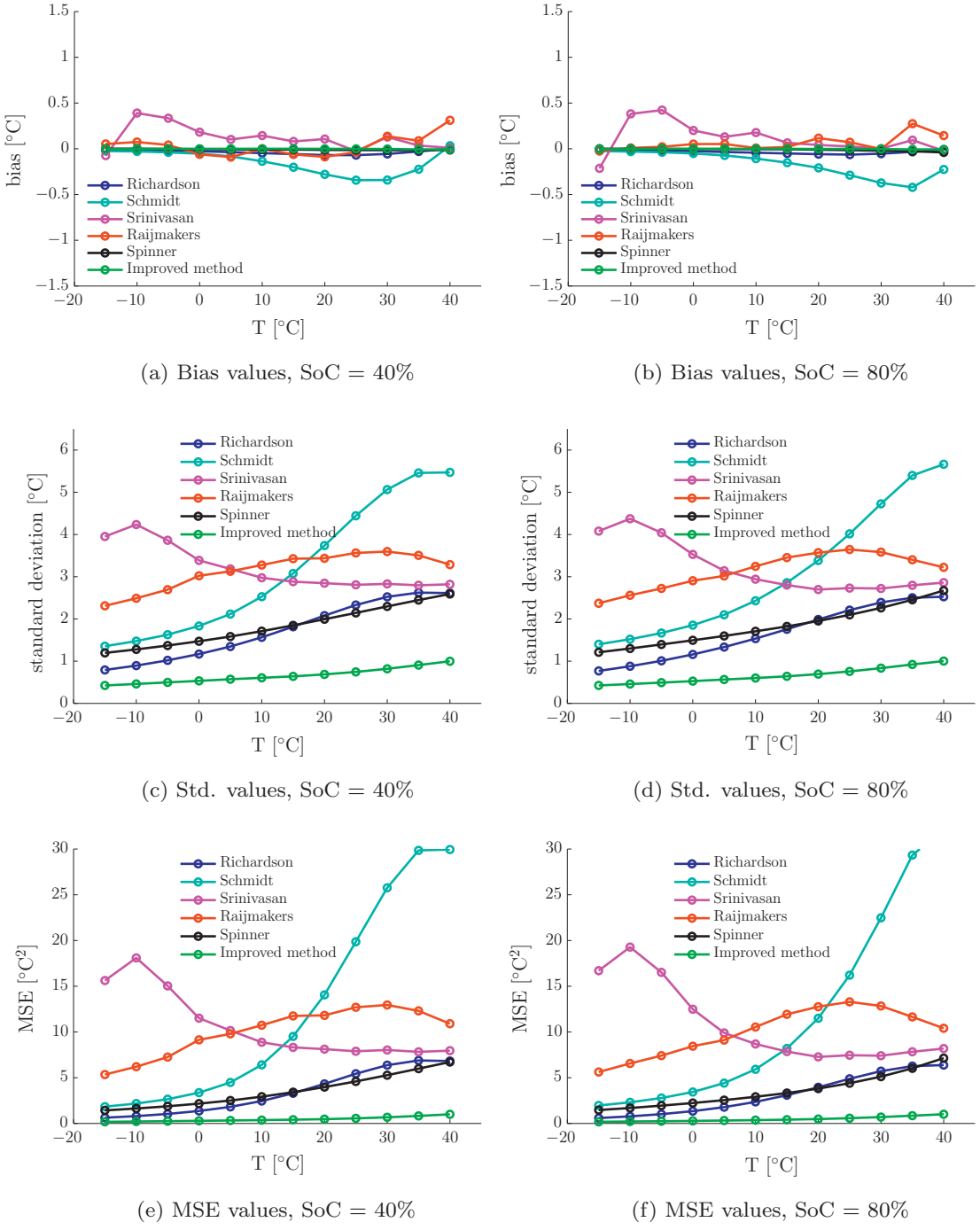

(a) Bias values, SoC = 40%

(b) Bias values, SoC = 80%

(c) Std. values, SoC = 40%

(d) Std. values, SoC = 80%

(e) MSE values, SoC = 40%

(f) MSE values, SoC = 80%

Fig. 8. Results of the comparison of estimation methods for case SoC known.

5.4. Results of the comparison

The results of the comparison of estimation methods, as defined in Table 1, are depicted in Fig. 7. In this figure, the plots show a comparison of bias values, standard-deviation values and MSE values in the top, middle and bottom plots, respectively. The left and right column show these results for SoC = 40% and SoC = 80%, respectively. In order to make a comparison, the estimation methods are evaluated at temperatures $T \in \{-15, -10, \ldots, +35, +40\}$ °C. Since the battery cell under investigation is not the same as the one used in [4,5,7–14], an equivalent frequency, complying with the description of the methods in Section 3.3, is chosen in the frequency spectrum of the $LiFePO_4$ cell. Also, the proposed improved method has been evaluated. For Fig. 7, the selected excitation frequencies can be found in Table 3. Furthermore, the results of the comparison are also shown in Table 3, Case A, in terms of the average absolute bias, the average standard deviation and the MSE, calculated over the same frequencies and temperatures as in Fig. 7 and $\text{SoC} \in \{20, 40, 60, 80\}\%$.

Based on these results, the improved method and the methods in [10,13] show the most accurate results in terms of overall bias and standard deviation for $\text{SoC} \in \{20, 40, 60, 80\}\%$, as well as in terms of the MSE in Fig. 7e and f. It should be noted that some methods yield better performance at high temperatures whilst other methods perform better at low temperatures. Therefore, the bias and average standard deviation do not give full details, but overall, the improved method outperforms the other methods.

6. Extensions

Besides the case presented in this paper, where the battery SoC is assumed to be unknown, the presented approach can be extended to situations where, for example, information on SoC and battery ageing [24,25] is incorporated. Also, the approach can be extended towards incorporating (dis)charge currents, such as drive currents in (hybrid) electric vehicles. These extensions can be interpreted as the effects w in the battery model in Eq. (7) and aim at improving the temperature estimate. An additional extension is to further investigate the effect of a non-uniform temperature distribution (i.e., a temperature gradient across the battery cell) on impedance-based temperature estimation, since the effect of temperature gradients on battery behaviour has been shown to be important in other studies, see, e.g., [26]. We will now present one particular extension, which is the incorporation of SoC in the temperature estimation. In this case, the model in Eq. (9) is used instead of Eq. (8) to do the temperature estimation in Eq. (10). Now, the SoC becomes an argument for the model in Eq. (9), comprising of a lookup-table for each SoC value in Table 2.

In Fig. 8 and Table 3, Case B, the results for the case where the SoC is known are shown in a similar way as for the case where the SoC is unknown in Fig. 7 and Table 3, Case A. The plots for standard deviation in Fig. 8c and d indicate that the standard deviation is not different from the case where the SoC is unknown. Table 3 confirms this. As to be expected, results for the bias are noticeably different compared to the case where the SoC is unknown. Now, the bias on the estimate is (very close to) zero as can be seen in Fig. 8a and b and Table 3, Case B. The overall accuracy in terms of the MSE in Fig. 8e and f, and Table 3, Case B, has slightly improved due to the improvement of the bias. Also, the improved method yields the best results in terms of MSE, however, the methods in [10,13] perform equally well in terms of bias. It can be argued that due to certain choices in experiment design, some estimation methods yield poorer performance than others for the case where the SoC is known.

A more qualitative interpretation of comparing the accuracy of the estimated battery temperature in the case where the SoC is known with the case where the SoC is unknown can also be given. In case of an unknown SoC, a typical approach is to use a battery model which has been averaged over a number of SoC or to use a model for a certain SoC value. Assuming that such a model will achieve the highest model accuracy around the centre of the SoC spectrum, i.e., SoC = 50%, temperature estimation in terms of bias on the estimate will most likely also be accurate around the centre of the spectrum. Moving away from the centre, towards the edges of the SoC spectrum, the battery model will become less accurate and the accuracy of the temperature estimate will also decrease accordingly. This is also supported by the quantitative findings in Figs. 5 and 6. For the case of a known SoC, the battery model will be equally accurate over the entire SoC range and therefore, the temperature estimate in terms of bias will be equally accurate over the entire SoC range.

7. Conclusions

For safety and control purposes, battery-temperature information is essential. Temperature estimation methods based on EIS can be broken down into two steps: choosing the excitation frequency f (i.e., experiment design) and estimating the temperature T based on the measured impedance Z (i.e., parameter estimation). This paper presents a novel, data-based approach in which experiment design and parameter estimation are combined in order to find the most accurate temperature estimate. Through the combination of these components, an improved and more accurate estimation method has been deduced. The estimation parameters within the approach can also be used to describe existing estimation methods. Given the fact that no prior knowledge of batteries or battery modelling is assumed, the framework is a promising tool for analysis of impedance-based temperature estimation.

Using experimental data from a Li-ion cell, the sensitivity of the battery impedance with respect to temperature and SoC is investigated and the accuracy of temperature estimates is analysed with a Monte-Carlo method for a large set of frequencies and temperatures. Results are evaluated in terms of bias, standard deviation and the MSE of the estimate $\hat{T}$. These results show that suitable estimation parameters can be found at low frequencies, using both the real and the imaginary part of the impedance. Also, a quantitative comparison of estimation methods, including the improved method, is performed. Overall, differences in choices of estimation parameters are found to result in significant differences between estimation methods. It has been verified that the improved method yields the best overall performance in terms of bias and standard deviation.

Acknowledgement

This work has received financial support from the Horizon 2020 programme of the European Union under the grant 'Integrated Components for Complexity Control in affordable electrified cars' (grant agreement no. 662192) and from the Dutch Ministry of Economic Affairs under the grant 'A green Deal in Energy Materials' (ADEM). Furthermore, the authors would like to thank Dr. Dmitry Danilov for valuable discussions.

References

[1] Beelen HPGJ, Raijmakers L, Donkers MCF, Notten PHL, Bergveld HJ. In: Proceedings of the 2015 IFAC workshop on engine and powertrain control, simulation and modeling, IFAC, Columbus, Ohio. p. 383–8. doi:10.1016/j.ifacol.2015.10.055.

[2] Balakrishnan PG, Ramesh R, Prem Kumar T. J Power Sources 2006;155:401–14. http://dx.doi.org/10.1016/j.jpowsour.2005.12.002.

[3] Feng X, Sun J, Ouyang M, He X, Lu L, Han X, Fang M, Peng H. J Power Sources 2014;272:457–67. http://dx.doi.org/10.1016/j.jpowsour.2014.08.094. URL: <http://dx.doi.org/10.1016/j.jpowsour.2014.08.09>.
[4] Richardson RR, Howey DA. IEEE Trans Sustainable Energy 2015;6:1190–9. http://dx.doi.org/10.1109/TSTE.2015.2420375.
[5] Raijmakers L, Danilov D, van Lammeren J, Lammers M, Notten P. J Power Sources 2014;247:539–44. http://dx.doi.org/10.1016/j.jpowsour.2013.09.005. URL: <http://linkinghub.elsevier.com/retrieve/pii/S0378775313014961>.
[6] Raijmakers L, Danilov D, van Lammeren J, Lammers M, Bergveld HJ, Notten P. IEEE Trans Ind Electron 2016;63(5):3168–78. http://dx.doi.org/10.1109/TIE.2016.2516961.
[7] Schmidt JP, Arnold S, Loges A, Werner D, Wetzel T, Ivers-Tiffée E. J Power Sources 2013;243:110–7. http://dx.doi.org/10.1016/j.jpowsour.2013.06.013. URL: <http://linkinghub.elsevier.com/retrieve/pii/S0378775313010070>.
[8] Srinivasan R, Carkhuff BG, Butler MH, Baisden AC. Electrochim Acta 2011;56:6198–204. http://dx.doi.org/10.1016/j.electacta.2011.03.136. URL: <http://linkinghub.elsevier.com/retrieve/pii/S0013468611005342>.
[9] Srinivasan R. J Power Sources 2012;198:351–8. http://dx.doi.org/10.1016/j.jpowsour.2011.09.077. URL: <http://linkinghub.elsevier.com/retrieve/pii/S0378775311018489>.
[10] Richardson RR, Ireland PT, Howey DA. J Power Sources 2014;265:254–61. http://dx.doi.org/10.1016/j.jpowsour.2014.04.129. URL: <http://dx.doi.org/10.1016/j.jpowsour.2014.04.129>.
[11] Zhu J, Sun Z, Wei X, Dai H. J Power Sources 2015;274:990–1004. http://dx.doi.org/10.1016/j.jpowsour.2014.10.182. URL: <http://linkinghub.elsevier.com/retrieve/pii/S0378775314018011>.
[12] Howey D, Mitcheson P, Yufit V, Offer G, Brandon N. IEEE Trans Veh Technol 2014;63:2557–66. http://dx.doi.org/10.1109/TVT.2013.2293597.
[13] Spinner NS, Love CT, Rose-Pehrsson SL, Tuttle SG. Electrochim Acta 2015;174:488–93. http://dx.doi.org/10.1016/j.electacta.2015.06.003. URL: <http://linkinghub.elsevier.com/retrieve/pii/S0013468615013602>.
[14] Koch R, Jossen A. In: 28th international electric vehicle symposium and exhibition (EVS28), Goyang, Korea.
[15] Orazem ME, Tribollet B. Electrochemical impedance spectroscopy. John Wiley & Sons; 2008.
[16] Barsoukov E, Macdonald JR. Impedance spectroscopy theory, experiment, and applications. John Wiley & Sons; 2005.
[17] Fleischer C, Waag W, Heyn H-M, Sauer DU. J Power Sources 2014;260:276–91. http://dx.doi.org/10.1016/j.jpowsour.2014.01.129. URL: <http://linkinghub.elsevier.com/retrieve/pii/S0378775314002249>.
[18] Fleischer C, Waag W, Heyn H-M, Sauer DU. J Power Sources 2014;262:457–82. http://dx.doi.org/10.1016/j.jpowsour.2014.03.046. URL: <http://linkinghub.elsevier.com/retrieve/pii/S0378775314003590>.
[19] Bergveld HJ, Kruijt WS, Notten PHL. Battery management systems: design by modelling. Eindhoven: Kluwer Academic Publishers; 2002.
[20] Buller S, Thele M, Karden E, Doncker RWD. J Power Sources 2003;113:422–30. http://dx.doi.org/10.1016/S0378-7753(02)00558-X.
[21] Barillas JK, Li J, Günther C, Danzer MA. Appl Energy 2015;155:455–62. http://dx.doi.org/10.1016/j.apenergy.2015.05.102.
[22] Rubinstein RY, Kroese DP. Simulation and the Monte Carlo method. 2nd ed. John Wiley & Sons; 2008.
[23] Yates RD, Goodman DJ. Probability and stochastic processes: a friendly introduction for electrical and computer engineers. 2nd ed. John Wiley & Sons; 2005.
[24] Vetter J, Novák P, Wagner MR, Veit C, Möller KC, Besenhard JO, Winter M, Wohlfahrt-Mehrens M, Vogler C, Hammouche a. J Power Sources 2005;147:269–81. http://dx.doi.org/10.1016/j.jpowsour.2005.01.006.
[25] Waag W, Käbitz S, Sauer DU. Appl Energy 2013;102:885–97. http://dx.doi.org/10.1016/j.apenergy.2012.09.030.
[26] Klein M, Tong S, Park JW. Appl Energy 2016;165:639–47. http://dx.doi.org/10.1016/j.apenergy.2015.11.090.